$S = \frac{1}{2}$ triangular-lattice antiferromagnets $Ba_3CoSb_2O_9$ and $CsCuCl_3$: Role of spin-orbit coupling, crystalline electric field effect, and Dzyaloshinskii-Moriya interaction

A. Sera,[1] Y. Kousaka,[1,2] J. Akimitsu,[1,2] M. Sera,[3] T. Kawamata,[4] Y. Koike,[4] and K. Inoue[1,2,5]

[1]*Graduate School of Science, Hiroshima University, Higashi-Hiroshima 739-8526, Japan*

[2]*Center for Chiral Science, Hiroshima University, Higashi-Hiroshima 739-8526, Japan*

[3]*Department of ADSM, Hiroshima University, Higashi-Hiroshima 739-8530, Japan*

[4]*Department of Applied Physics, Tohoku University, Sendai 980-8579, Japan*

[5]*IAMR, Hiroshima University, Higashi-Hiroshima 739-8526, Japan*

(Received 20 June 2016; revised manuscript received 11 November 2016; published 8 December 2016)

We have performed the detailed investigations of the magnetization of the $S = \frac{1}{2}$ triangular-lattice antiferromagnets $Ba_3CoSb_2O_9$ and $CsCuCl_3$ with a 120° spin structure in the *ab* plane. In $Ba_3CoSb_2O_9$, the magnetic susceptibility (χ) exhibits a broad maximum above the Néel temperature (T_N) as is expected in the low-dimensional antiferromagnet (AFM). In $CsCuCl_3$, χ exhibits a continuous increase down to T_N as if it is the three-dimensional AFM. This is induced by the strong ferromagnetic (FM) interaction along the *c* axis. The magnetic phase diagrams are also very different. Although the transition field from the umbrella to the 2-1-coplanar phase ($H_{u\text{-}c}$) for $H \parallel c$ is almost independent of temperature in $Ba_3CoSb_2O_9$, it shows a considerable decrease with increasing temperature in $CsCuCl_3$. The temperature independent $H_{u\text{-}c}$ in $Ba_3CoSb_2O_9$ originates from the magnetic anisotropy from the van Vleck contribution, which does not depend so much on the temperature. The temperature dependent $H_{u\text{-}c}$ in $CsCuCl_3$ originates from the magnetic anisotropy from the Dzyaloshinskii-Moriya (DM) interaction, which decreases with increasing temperature. For $H \parallel ab$, the clear transition from the Y-coplanar to the *up-up-down* (*uud*) phase was observed in $Ba_3CoSb_2O_9$ but not in $CsCuCl_3$. While the reentrant behavior of T_N originating from the thermal and quantum spin fluctuations is observed in both compounds, it is pronounced in $Ba_3CoSb_2O_9$ but small in $CsCuCl_3$. These differences originate from the existence or nonexistence of the DM interaction. The DM interaction in $CsCuCl_3$ suppresses those fluctuations in the *ab* plane, leading to the less pronounced reentrant behavior of T_N and the broad crossover in place of the phase transition. We analyzed the anisotropic magnetization of $Ba_3CoSb_2O_9$ in the paramagnetic region by the mean field calculation. The spin-orbit (SO) coupling, the uniaxial crystalline electric field, and the isotropic exchange interaction were taken into account. We could estimate the anisotropy ratio of the exchange interaction $J/J_z = 1.19$ and $g_\perp/g_\parallel = 1.13$ with $g_\perp = 4.45$ and $g_\parallel = 3.95$ in the ground state. We emphasized that although the isotropic exchange interaction was used, the above anisotropies at low temperatures are induced simultaneously through the SO coupling and the uniaxial crystalline electric field and they are closely associated with each other.

DOI: 10.1103/PhysRevB.94.214408

I. INTRODUCTION

Elucidation of the ground state of frustrated quantum magnets is a key issue in condensed matter physics [1,2]. When the spin is $S = \frac{1}{2}$, the various types of exotic ground state could be realized due to the strong quantum frustration. One is the quantum spin-liquid ground state. Another is the magnetic order in the triangular-lattice antiferromagnet (TLA) with a 120° spin structure [3–8]. The classical ground state of the TLA is infinitely degenerate in magnetic field, where even very small perturbations can play a crucial role in exotic magnetic ordering. The theoretical studies have been performed to elucidate how the degeneracy is lifted by the thermal and quantum spin fluctuations. The *up-up-down* (*uud*) ground state providing a $M_s/3$ plateau (M_s is the saturation magnetization) is well known as a typical exotic ground state dominated by such fluctuation effects. However, only few compounds showing the *uud* ground state are known because of the difficulty in designing such compounds from a synthetic point of view.

$CsCuCl_3$, Cs_2CuBr_4, and $Ba_3CoSb_2O_9$ are known as the $S = \frac{1}{2}$ triangular-lattice compounds accompanied with the quantum phase transition.

Cs_2CuBr_4 has an orthothorhombic crystal structure with a space group $Pnma$. Although the triangular lattice is formed in the *bc* plane, it is irregular. Furthermore, there exist the Dzyaloshinskii-Moriya (DM) interactions [9,10]. Thus, although the *uud* phase was discovered, the analysis is very difficult and the microscopic mechanism has not yet been clarified [11].

$CsCuCl_3$ is the first compound in which the appearance of the quantum phase transition was confirmed [12–14]. The crystal structure of $CsCuCl_3$ at high temperatures is hexagonal with a space group $P6_3/mmc$ and the $CuCl_6$ octahedra form the chains along the *c* axis by sharing faces. Below 423 K, the crystal structure is changed to that with a space group $P6_122$ or $P6_522$ [15–17]. This structural phase transition is induced by the Jahn-Teller effect. In the low-temperature phase, Cu chains along the *c* axis form the helices along the *c* axis with a six periodicity. However, the regular triangular lattice in the *ab* plane is maintained and a 120° spin structure is realized below $T_N = 10.7$ K [17,18]. The magnetic properties have been studied extensively [12,13,17–22]. The exchange interaction along the *c* axis (J_{ex}^c) is strongly ferromagnetic (FM). It is estimated as large as ∼28 K. These one-dimensional chains form the

regular triangular lattice in the ab plane and are coupled with the AFM interaction with $J_{ex}^{ab} \sim -5$ K. The chirality of the Cu chains allows the DM interaction with $\boldsymbol{D}$ vector pointing the chain. Its strength is estimated to be $D \sim 5$ K. Below T_N, this compound exhibits a helical magnetic order along the c axis with a long period. This magnetic structure originates from the competition between the FM and the DM interactions. The resultant spin configuration is helical with a periodicity of $11.8c$ along the c axis and the spins between the nearest planes are rotated by 5.1° [18]. In the magnetization curve for $H \parallel c$, a discontinuous jump was discovered at 12.5 T [12,13]. Nikuni and Shiba demonstrated that this unexpected small magnetization jump for $H \parallel c$ originated from the quantum phase transition from the umbrella to the 2-1-coplanar phase. There, the thermal and quantum spin fluctuations play an essential role [14]. The magnetic properties for $H \parallel ab$ were also investigated in details. The magnetization exhibits a broad plateau between 10 and 14 T [13]. The detailed investigations by the neutron diffraction also have been performed [23,24]. However, the microscopic origin of the broad plateau has not yet been clarified [25,26]. Recently, this compound attracted attention from the standpoint of the chirality of the crystal structure [27,28].

Recently discovered $Ba_3CoSb_2O_9$ has a hexagonal crystal structure with a space group $P6_3/mmc$ [29]. This is the same as that in the high-temperature phase in $CsCuCl_3$. Since the discovery of the $M_s/3$ plateau in the magnetization curve [30], this compound has been studied extensively because this compound was considered as the ideal $S = \frac{1}{2}$ Heisenberg TLA and the comparison with the theoretical analysis was possible [30–37]. In the ab plane, the regular triangular lattice is formed and a 120° spin structure is realized below $T_N = 3.8$ K [29]. For $H \parallel ab$, the transition from the Y-coplanar to the uud phase appears at 9.5 T and the transition from the uud to the 2-1-coplanar phase at 15 T. For $H \parallel c$, the transition from the umbrella to the 2-1-coplanar magnetic phase takes place at 12.5 T [32]. The ground state of Co^{2+} ion in the octahedral environment could be reduced to the effective spin $S_{eff} = \frac{1}{2}$ system due to the spin-orbit coupling with a uniaxial crystalline electric field. This compound has a regular triangular lattice and the distance between the nearest ab plane is as large as 7.2 Å and the planes are separated by the nonmagnetic Sb_2O_9 double octahedral and Ba^{2+} ions. Thereby, the antiferromagnetic (AFM) interplane coupling, i.e., the AFM interaction along the c axis is as weak as -0.5 K. On the other hand, the intraplane AFM interaction is strong and is estimated to be -18 K. Thus, the quasi-two-dimensional magnetic system is realized. A broad maximum of the magnetic susceptibility little above T_N is a sign of a low-dimensional magnetic system. The magnetic phase diagrams were studied in details by specific heat, magnetization, and ultrasonic measurements [31,33]. For $H \parallel ab$, T_N increases up to 5.3 K at 13 T and decreases above this field. Thus, a pronounced reentrant behavior of T_N is observed in the uud phase. At $H = 22$ T for $H \parallel ab$, another type of the phase transition was discovered [32]. This transition has attracted much attention and the theoretical studies have been performed extensively [35,36]. The magnon dispersion was also studied by the inelastic neutron scattering and was analyzed theoretically [37]. The thermal conductivity κ was investigated to clarify the dynamic nature of the spin fluctuation and it was found that κ shows the largest suppression at $\sim$13 T, which is the middle in the uud phase [34].

In this paper, we performed the detailed studied of the magnetic properties of $CsCuCl_3$ and $Ba_3CoSb_2O_9$ to clarify the effect of the orbital momentum on the anisotropy of the ground state of TLA. The reason why we compare these two compounds is that the contributions of the orbital degrees of freedom are quite different. In the ground state of $CsCuCl_3$, the orbital momentum is almost quenched and a small relived orbital momentum through the excited states contributes to the DM interaction. The DM interaction works as the magnetic anisotropy to fix the spins in the ab plane. In the ground state of $Ba_3CoSb_2O_9$, the contribution of the orbital momentum through the van Vleck term is not small. At the early stage, $Ba_3CoSb_2O_9$ was considered as the ideal $S = \frac{1}{2}$ Heisenberg TLA. However, the recent theoretical analysis suggests the existence of the considerable magnitude of anisotropy in the exchange interaction [35–37]. The anisotropy of the exchange interaction might originate from the orbital degrees of freedom in Co^{2+} ion. Then, the orbital degrees of freedom should be taken into account seriously in the analysis of the magnetic properties of the Co compounds. In this paper, we performed the mean field calculation for $Ba_3CoSb_2O_9$, focused on the magnetic properties in the paramagnetic region at the high temperatures and high magnetic fields to clarify the effect of the orbital degrees of freedom on the ground state. In such a paramagnetic region, the effect of the thermal and quantum spin fluctuations is negligible. Since the orbital momentum couples with the lattice, the anisotropic property of the g factor and the exchange interaction are expected to be affected by pressure. Then, the present studies of the two compounds with different contribution of the orbital momentum could be the guide to the study of the pressure effect on the thermal and quantum spin frustrations in the TLA.

II. EXPERIMENT

Single crystals of $Ba_3CoSb_2O_9$ were grown by the floating-zone method [34]. Single crystals of $CsCuCl_3$ were grown from a slightly acidified solution containing CsCl and $CuCl_2 \cdot 2H_2O$ by evaporation of solvent [18]. The magnetization was measured using a Quantum Design MPMS-5S magnetometer up to 5 T and the extraction method up to 14.8 T. A good quality of the present sample is verified by a sharp specific-heat peak at T_N. A peak height of the specific heat C/T at $H = 0$ is 6.3 $J/K^2/mol$ and a peak at T_N is very sharp. A sharp discontinuous jump is seen in the M-H curve at $H = 12.5$ T for $H \parallel c$, which will be shown in Fig. 3. These results indicate a good quality of the single crystal $Ba_3CoSb_2O_9$ used in this paper. The quality of $CsCuCl_3$ single crystal is also good judging from a sharp discontinuous jump of M-H curve for $H \parallel c$, which will be shown in Fig. 8. We measured the magnetization of both samples by rotating the magnetic field in the ac plane and the sample orientation in magnetic field was found to be good. The magnetic susceptibility up to 300 K was measured with increasing temperature. In the other cases, it was measured with decreasing temperature. The samples were cooled in zero field, in principle. We could not

observe a hysteresis at the first-order phase transition within an experimental accuracy.

III. EXPERIMENTAL RESULTS

A. $Ba_3CoSb_2O_9$

1. Magnetization at low magnetic fields

The temperature (T) dependencies of χ_{ab} and χ_c of $Ba_3CoSb_2O_9$ are shown in Figs. 1(a) and 1(b). Here, χ_{ab} and χ_c are the magnetic susceptibilities for $H \parallel ab$ and $H \parallel c$, respectively. A large anisotropy is observed in a wide range of temperature. Both χ_{ab} and χ_c exhibit a Curie-Weiss behavior at high temperatures as seen in Fig. 1(a). The paramagnetic Curie temperature (θ_p) is -60 and -90 K for $H \parallel ab$ and $H \parallel c$, respectively. χ_{ab} and χ_c deviate from the Curie-Weiss behavior below $\sim$200 K and exhibit a broad maximum at $T_{max} \sim 7$ K. T_{max} could be very rough estimation of the AFM interaction in the ab plane. In the paramagnetic region, a large anisotropy exists in the magnetic susceptibility. $\chi_{ab} > \chi_c$; $\chi_{ab}/\chi_c = 1.19$ and 1.12 at 7 and 300 K, respectively. Such a large magnetic anisotropy continues to exist also below T_N. Both χ_{ab} and χ_c measured at low magnetic field exhibit the small anomalies at $T_N = 3.8$ K. In a low magnetic field region below T_N, the Y-coplanar and the umbrella phases are realized for $H \parallel ab$ and $H \parallel c$, respectively, as was reported previously [31–33]. A decrease of χ below T_N is larger for $H \parallel ab$ than for $H \parallel c$. In the umbrella phase, the three spins are canted to $H \parallel c$, χ_c follows the similar T dependence to $\chi_\perp$ expected in a usual antiferromagnet. For $H \parallel ab$, χ below T_N includes both components of $\chi_\perp$ and $\chi_\parallel$. Thus, a larger decrease is expected in χ_{ab} than in χ_c below T_N. A small continuous decrease through T_N in both χ_{ab} and χ_c might originate from the two-dimensional spin fluctuation.

χ_{ab} exhibits a broad maximum at $T_{max} \sim 7$ K. This maximum becomes less pronounced with increasing magnetic field. It is because the magnitude of χ_{ab} increases rapidly with increasing magnetic field and the maximum disappears at $\sim$5 T as is seen in Fig. 2(a). The results are, in principle, the same as those reported previously [31]. This H dependence of χ_{ab}-T curve means the pronounced concave H dependence of the M_{ab}-H curve in a temperature region up to $\sim$7 K. Here, M_{ab} is the magnetization for $H \parallel ab$. The concave H dependence of the M_{ab}-T curve above T_N originates from the existence of the uud phase at higher magnetic fields between 4 and 5.3 K as will be shown in Fig. 5(a). In the uud phase below 13 T, M_{ab} exhibits an increase below T_N, which will be shown in Fig. 4(a). This suggests that a pronounced concave H dependence of the M_{ab}-H curve in the paramagnetic region below $\sim$6 K originates from the short-range order (SRO) effect. This is supported by a large tail of specific heat (C) above T_N in the uud phase [31]. Thus, the thermal and quantum fluctuations exist as the SRO effect in this temperature region above T_N. Around T_N, χ_{ab} exhibits the two anomalies, i.e., a dip and a peak. Although its separation is very small at low magnetic fields, it increases with increasing magnetic field, as is seen in Fig. 2(b).

In contrast to the case of $H \parallel ab$, a maximum of χ_c at $T_{max} \sim 7$ K remains even at 5 T since the H dependence of the χ_c-T curve is small below 7 K. As is shown in Fig. 2(c), this indicates that although the M-H curve shows a slightly concave H dependence, it is small and M_c shows a roughly H-linear increase in this temperature region. In contrast to a large tail of C above T_N in the uud phase for $H \parallel ab$, it is

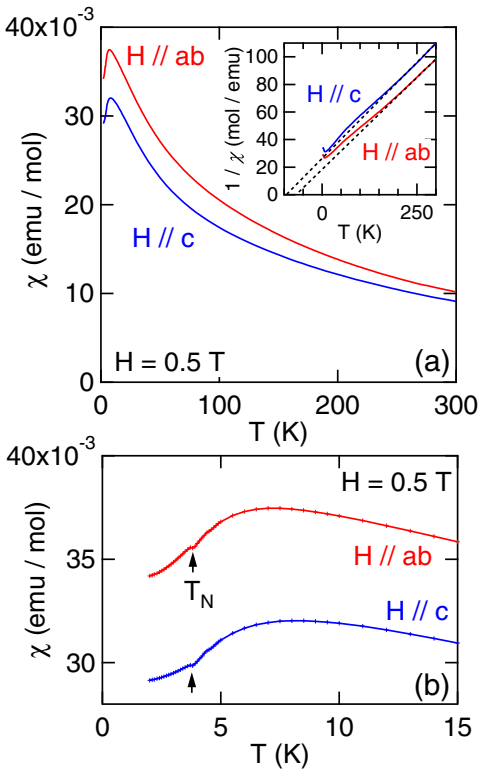

FIG. 1. (a) Temperature dependence of the magnetic susceptibility of $Ba_3CoSb_2O_9$ for $H \parallel ab$ and $H \parallel c$ measured at $H = 0.5$ T. The inset exhibits the temperature dependence of the inverse magnetic susceptibility. The dotted lines are drawn to estimate the paramagnetic Curie temperature (θ_p). (b) Magnetic susceptibilities in an expanded scale below 15 K.

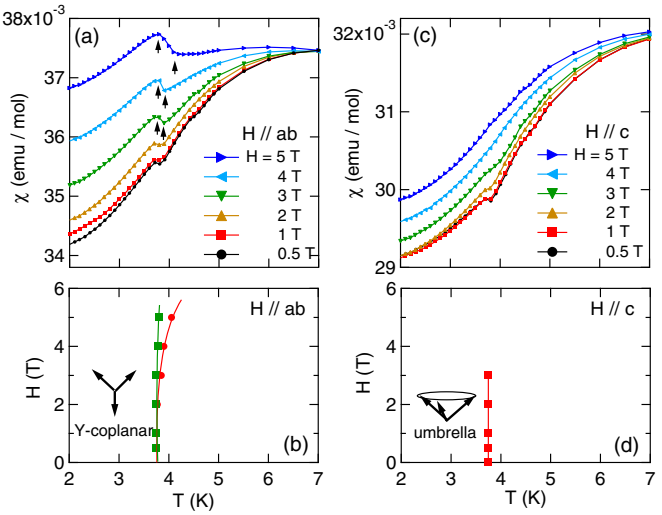

FIG. 2. Temperature dependence of the magnetic susceptibility of $Ba_3CoSb_2O_9$ for (a) $H \parallel ab$ and (c) $H \parallel c$ at various magnetic fields up to 5 T. The arrows in (a) indicate the transition temperature. Magnetic phase diagrams for (b) $H \parallel ab$ and (d) $H \parallel c$ obtained from the magnetic susceptibility data.

much smaller for $H \parallel c$ [31]. This is due to the small SRO effect above T_N in the umbrella phase. Thus, the effect of the thermal and spin fluctuations above T_N is different between the *uud* and the umbrella phases. Around at T_N, a dip and peak are observed in low magnetic field up to 2 T. However, both are not recognized above 4 T as is seen in Fig. 2(d).

2. *Magnetization at high magnetic fields*

The M-H curves of $Ba_3CoSb_2O_9$ at $T = 1.5$ K for $H \parallel ab$ and $H \parallel c$ are shown in Fig. 3. The results are similar to the previous one [32]. The anomaly of M_c at $H_{u\text{-}c}$ is much sharper in the present result than in the previous one [32]. M_{ab} shows a pronounced concave H dependence up to $H_{Y\text{-}uud} \sim 9.5$ T and above $H_{Y\text{-}uud}$, a slope of M_{ab}/H is small. Here, $H_{u\text{-}c}$ and $H_{Y\text{-}uud}$ are the transition field from the umbrella to the 2-1-coplanar phase and from the Y-coplanar to the *uud* phase, respectively. The $M_s/3$ plateau in the *uud* phase has a small finite slope of M_{ab}/H, originating from the van Vleck contribution. The characteristic M-H curves were reproduced by the theoretical investigations [35,36]. On the other hand, M_c exhibits nearly H-linear increase up to $H_{u\text{-}c} = 12$ T. This is consistent with a small increase of χ_c with increasing magnetic field at low temperatures as is seen in Fig. 2(c). The H-linear M-H curve is expected in the umbrella phase because the spin-canting magnetization process is realized. At $H_{u\text{-}c}$, a discontinuous jump of $M(\Delta M)$ is seen, which was not observed in the previous paper [32]. Above $H_{u\text{-}c}$, a concave H dependence is observed. These characteristic H dependencies of M_c were reproduced theoretically [36]. We note that there exists a rather large magnetic anisotropy of $M_{ab} > M_c$ in the AFM ordered phase.

Figure 4(a) represents the T dependence of M_{ab} above 5 T. A broad maximum of M_{ab} at $T_{max} \sim 7$ K disappears above 6 T and the T dependence of M_{ab} is changed to a monotonous increase with decreasing temperature. Between 6 and 8 T, M_{ab} exhibits an increase below T_N and after showing a peak at $T_{Y\text{-}uud}$, it decreases with decreasing temperature. Here, $T_{Y\text{-}uud}$ is the transition temperature from the Y-coplanar to the *uud* phase. $T_{Y\text{-}uud}$ shifts to lower temperature with increasing magnetic field. On the other hand, T_N increases with increasing

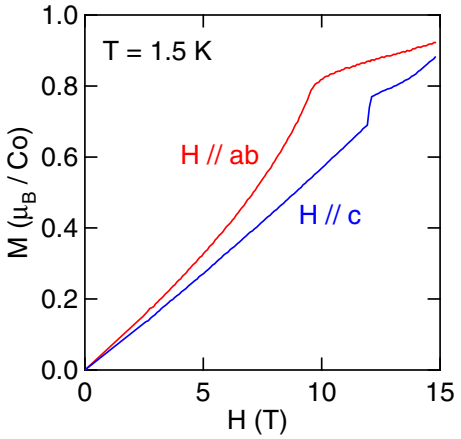

FIG. 3. Magnetization curves of $Ba_3CoSb_2O_9$ at $T = 1.5$ K for $H \parallel ab$ and $H \parallel c$.

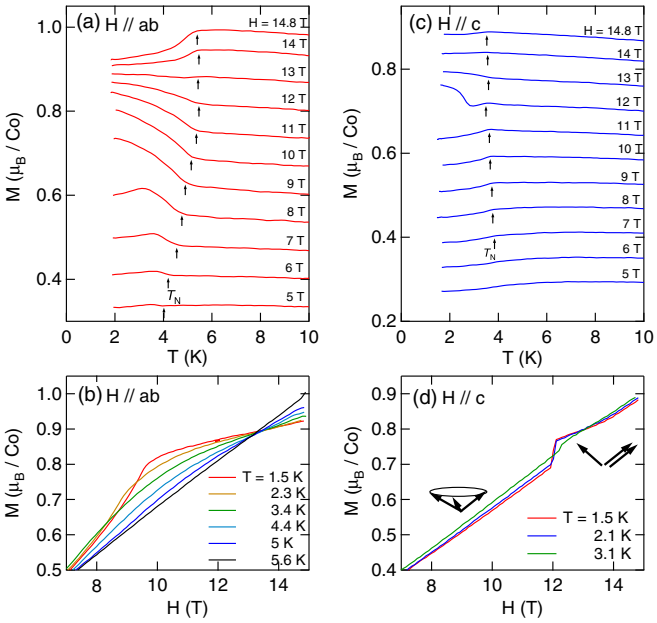

FIG. 4. Temperature dependence of the magnetization of $Ba_3CoSb_2O_9$ for (a) $H \parallel ab$ and (c) $H \parallel c$ at various magnetic fields up to 14.8 T. Magnetization curves of $Ba_3CoSb_2O_9$ for (b) $H \parallel ab$ and (d) $H \parallel c$ at various temperatures.

magnetic field up to 13 T. After showing a maximum value of 5.3 K at ~13 T, T_N decreases with increasing magnetic field above this field. Thus, the magnetic phase diagram exhibits the reentrant behavior of T_N in the *uud* phase. The M-H curve for $H \parallel ab$ exhibits a plateau with a small finite slope of M_{ab}/H in the *uud* phase at 1.5 K. With increasing temperature, the slope is enhanced rapidly and a kink at $H_{Y\text{-}uud}$ is rapidly smeared out. As is shown in Fig. 4(b), the M-H curves below T_N coincide with each other at 13.2 T. This corresponds to the almost temperature-independent M-T curve at 13 T in Fig. 4(a). Above 14 T, M_{ab} decreases below T_N. This is consistent with the decrease of T_N with increasing magnetic field.

For $H \parallel c$, although the anomaly at T_N is difficult to recognize below 6 T, a kink is observed at T_N above 7 T as is seen in Fig. 4(c). This kink is changed to a peak above 9 T and is clearly seen up to 12 T. In this field region, T_N decreases slightly with increasing magnetic field. At 12 T, another anomaly, i.e., a discontinuous increase ΔM_c appears below ~3 K. This originates from the transition from the umbrella to the 2-1-coplanar phase. At 13 T, M_c exhibits a small increase below T_N. M_c is nearly constant below T_N at 14 T and decreases below T_N at 14.8 T. The M-H curve shows a jump ΔM at $H_{u\text{-}c} = 12$ T as is seen in Fig. 4(d) and it is rapidly smeared out with increasing temperature above $T \sim 2$ K. Above $H_{u\text{-}c}$, M_c exhibits a concave H dependence.

The magnetic phase diagrams of $Ba_3CoSb_2O_9$ for $H \parallel ab$ and $H \parallel c$ are shown in Figs. 5(a) and 5(b), respectively. The reentrant behavior of T_N is observed in the *uud* phase. Along a black dashed line in Fig. 5(a), the quantum spin and thermal fluctuations might work most effectively, judging from the highest T_N. In the $S = \frac{1}{2}$ Heisenberg TLA, the magnetic structure in magnetic field has the infinite degeneracies within a classical theory, but these degeneracies are lifted by the

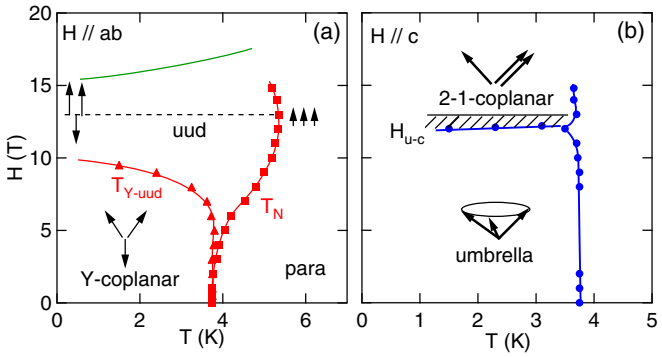

FIG. 5. (a) Magnetic phase diagram of $Ba_3CoSb_2O_9$ for $H \parallel ab$. Green line indicates the transition field from *uud* to coplanar state, which is cited from Ref. [36]. Along a black dashed line, the thermal and quantum spin fluctuation works most effectively, where T_N is the highest. (b) Magnetic phase diagram for $H \parallel c$. In the hatched area, T_N increases with increasing magnetic field, which might be due to the larger effect of the thermal and quantum spin fluctuation than the Zeeman effect.

quantum spin fluctuation and also by the thermal fluctuation. At finite temperatures, the infinitely degenerate configurations in magnetic field are lifted mainly by the thermal fluctuation, i.e., the entropy effect [6,7]. The collinear structure is most favorably stabilized, next the coplanar one, and finally the noncoplanar one. T_N in the *uud* phase increases with increasing magnetic field up to $H = 13$ T, i.e., $dT_N/dH > 0$. This indicates that the magnetic entropy in the *uud* phase is larger than that in the paramagnetic phase. When T_N is the highest, the energy gain by the entropy effect is expected to be the largest. Above $H = 13$ T, the Zeeman energy gain overcomes the entropy effect and T_N is reduced. The slightly reentrant behavior of the magnetic phase diagram was observed also in $CsCuCl_3$. There, the importance of the thermal fluctuation was emphasized [22]. We note that the reentrant behavior of T_N in the *uud* phase was obtained by the Monte Calro simulation [6]. Just above T_N at 13 T, the magnitude of the induced moment is $\sim M_s/3$ in all the Co^{2+} ion site. This is shown schematically by the three small arrows in Fig. 5(a). With decreasing temperature, two of them increase up to M_s and one of them decreases and is reduced to $-M_s$. Above 13 T, for example, at 14 T, the moment of each Co^{2+} ion just above T_N is larger than $M_s/3$ but at $T = 0$ K, the average moment of the three sublattices is $\sim M_s/3$. Thus, M_{ab} exhibits a peak at T_N. Below 13 T, for example, at 11 T, the moment of each Co^{2+} ion just above T_N is smaller than $M_s/3$. However, at $T = 0$ K, the average moment of the three sublattices is $\sim M_s/3$. Thus, M_{ab} exhibits an increase below T_N. Above the green line, a coplanar phase different from the 2-1-one is known to be realized [35,36]. Here, we briefly comment the minimum of κ at $\sim$13 T [34]. The thermal current is carried by phonon, magnon, or both. In any case, the minimum of κ means the shortest mean-free path of phonon or magnon at this magnetic field. There, the collision of phonon or magnon with the thermal and quantum spin fluctuations should play the important role.

Finally, we comment the slightly different magnetic phase diagram for $H \parallel ab$ between the present result and those

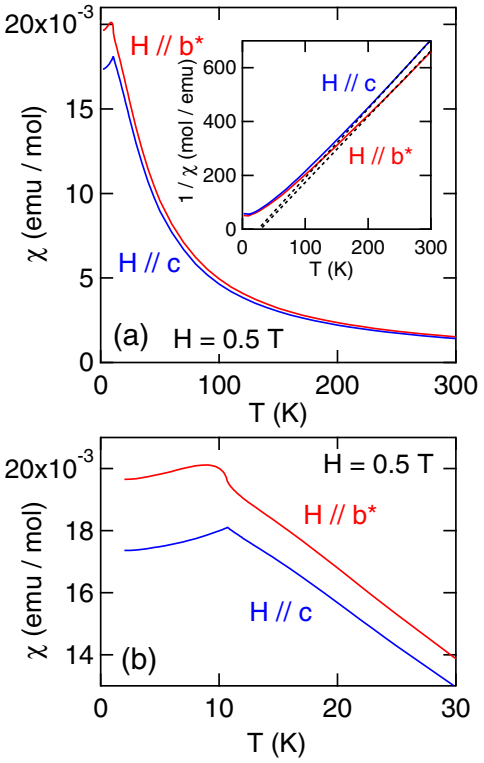

FIG. 6. (a) Temperature dependence of the magnetic susceptibility of $CsCuCl_3$ for $H \parallel b^*$ and $H \parallel c$. The inset shows the temperature dependence of the inverse magnetic susceptibility. The dotted lines in the inset are drawn to estimate the paramagnetic Curie temperature. (b) Magnetic susceptibilities in an expanded scale below T_N.

reported previously [31,33]. The difference is seen in the phase boundary around the tricritical point. It is $\sim$3 T in the present result and $\sim$6 T in those reported previously [31,33]. We should note that the present data are almost the same as the previous ones [31,33]. A peak temperature of χ_{ab} is also the same in both results. In the previous papers, a peak temperature was used to construct the magnetic phase diagram. On the other hand, we took the higher-temperature anomaly above the lower T_N as the transition temperature. This is shown by the arrows in Fig. 2(a). Thus, the magnetic phase diagram for $H \parallel ab$ around the tricritical point is slightly different between the present result and previous ones. The position of the tricritical point is important to understand the nature of the thermal and quantum spin fluctuations in the TLA and should be clarified in the future.

For $H \parallel c$, the H dependence of T_N for $H \parallel c$ is much smaller than that for $H \parallel ab$. In the hatched area, the thermal and quantum spin fluctuations are active, which will be discussed later. The T dependence of $H_{u\text{-}c}$ is very small. This contrasts to the large T dependence of $H_{u\text{-}c}$ in $CsCuCl_3$, which will be shown later.

B. $CsCuCl_3$

1. *Magnetization at low magnetic fields*

Figure 6(a) represents the T dependence of χ of $CsCuCl_3$ for $H \parallel b^*$ and $H \parallel c$ and Fig. 6(b) those in the expanded scale below 30 K. Here, b^* is located in the ab plane and is

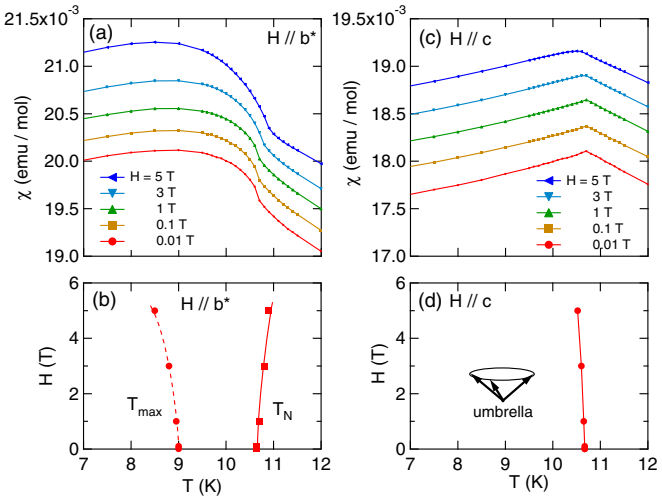

FIG. 7. Temperature dependence of the magnetic susceptibility of $CsCuCl_3$ for (a) $H \parallel b^*$ and (c) $H \parallel c$ at various magnetic fields up to 5 T. The origin of the vertical axis is shifted in each χ-T curve. Magnetic phase diagrams for (b) $H \parallel b^*$ and (d) $H \parallel c$ obtained by the temperature dependence of the magnetic susceptibility.

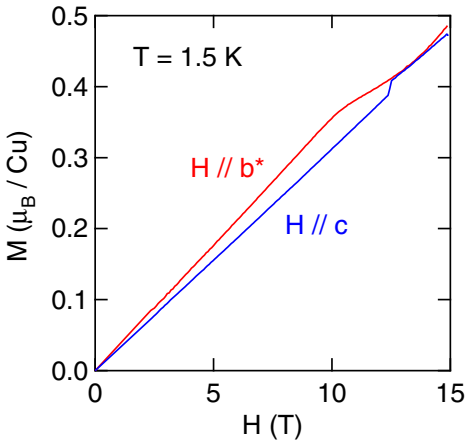

FIG. 8. Magnetization curves of $CsCuCl_3$ for $H \parallel b^*$ and $H \parallel c$ at $T = 1.5$ K.

perpendicular to the ac plane. The inset of Fig. 6(a) represents the T dependence of χ^{-1}. While χ of the single crystal was reported before [17,20], the detailed behaviors around T_N were not studied. We note that although χ_c exhibits a decrease below T_N as in a usual antiferromagnet, χ_{b^*} exhibits a pronounced increase below T_N and a broad maximum at slightly below T_N. The continuous increase of χ of $CsCuCl_3$ with decreasing temperature in the paramagnetic region is very different from that of the typical two-dimensional AFM compound accompanied with a broad maximum above T_N. Furthermore, a positive θ_p is as large as ~20 K. This is different from a large negative θ_p in $Ba_3CoSb_2O_9$. This unusual T dependence of χ should originate from the strong FM interaction along the c axis, which dominates the magnetic properties in the paramagnetic region. χ^{-1} exhibits a deviation from the Curie-Weiss behavior below ~100 K. This might originate from the two-dimensional spin fluctuation. The anisotropy of χ in the paramagnetic region exists also in $CsCuCl_3$. However, $\chi_{b^*}/\chi_c = 1.07$ at $T = 20$ K is much smaller than 1.19 of $Ba_3CoSb_2O_9$ at the same temperature. On the other hand, χ_{b^*}/χ_c below T_N is as large as 1.13. This is associated with the enhancement of χ_{b^*} below T_N, which is observed only for $H \parallel b^*$. On the other hand, in $Ba_3CoSb_2O_9$, both χ_{ab} and χ_c show the similar T dependence below T_N and the magnitude of the anisotropy of χ is independent of the temperature below and above T_N.

χ_{b^*} exhibits a large enhancement below T_N and a broad maximum at $T_{max} \sim 9$ K as seen in Fig. 7(a). With increasing magnetic field, the enhancement of χ_{b^*} below T_N increases and T_{max} shifts to lower temperature. T_N increases slightly with increasing magnetic field up to 5 T. T_{max} decreases from ~9 K at $H = 0$ T down to ~8.5 K at 5 T as is seen in Fig. 7(b).

For $H \parallel c$, T_N decreases slightly with increasing magnetic field, as is seen in Fig. 7(d). χ_c shows a sharp peak at T_N at low magnetic fields. However, a sharpness of a peak is suppressed with increasing magnetic field. At 5 T, χ_c exhibits only a rounded peak at T_N. This might originate from the fact that 5 T is close to the transition field of $H_{u\text{-}c} \sim 6$ T. Namely, the effect of the thermal and quantum spin fluctuations in the 2-1-coplanar phase might appear in this field region.

2. *Magnetization at high magnetic fields*

Figure 8 exhibits the M-H curves of $CsCuCl_3$ at 1.5 K for $H \parallel b^*$ and $H \parallel c$. The results are nearly the same as those reported previously [13]. M_c exhibits nearly H-linear increase up to $H_{u\text{-}c} = 12.5$ T and a small discontinuous jump ΔM at this field. The H-linear M-H curve up to $H_{u\text{-}c}$ originates from the spin canting magnetization process in the umbrella phase. M_{b^*} also shows nearly H-linear increase up to ~10 T and after showing a shoulder at ~10 T, M_{b^*} increases with a concave H dependence above ~11 T. A large magnetic anisotropy of $M_{b^*} > M_c$ exists up to 12.5 T. However, it is small at high magnetic fields. This is different from the large magnetic anisotropy in $Ba_3CoSb_2O_9$ up to 14.8 T as is seen in Fig. 3.

Figure 9(a) represents the T dependence of M_{b^*}. M_{b^*} exhibits an increase below T_N in magnetic field up to 8 T and a broad maximum at T_{max} little below T_N. T_{max} shifts to lower temperature with increasing magnetic field. Above 9 T, M_{b^*} exhibits a peak at T_N. As is shown in Fig. 9(b), the M-H curve for $H \parallel b^*$ exhibits nearly H-linear increase up to ~10 T. Around this field, a shoulder is observed. This is very different from the pronounced concave H dependence of M_{ab} up to $H_{Y\text{-}uud}$ in $Ba_3CoSb_2O_9$. A broad plateau between 10 and 14 T is smeared out with increasing temperature. The magnetic field of a shoulder shifts to lower magnetic field with increasing temperature.

In contrast, M_c shows a peak at T_N at low magnetic field. T_N is reduced slightly with increasing magnetic field up to 6 T. Between 6 and 9 T, a peak at T_N disappears and in place, M_c slightly increases below T_N with decreasing temperature. Here, T_N increases slightly with increasing magnetic field. This might originate from the enhancement of the thermal and quantum spin fluctuations, which will be discussed later. Above 10 T, a peak appears again at T_N and T_N decreases with increasing magnetic field. Above 6 T, another phase transition

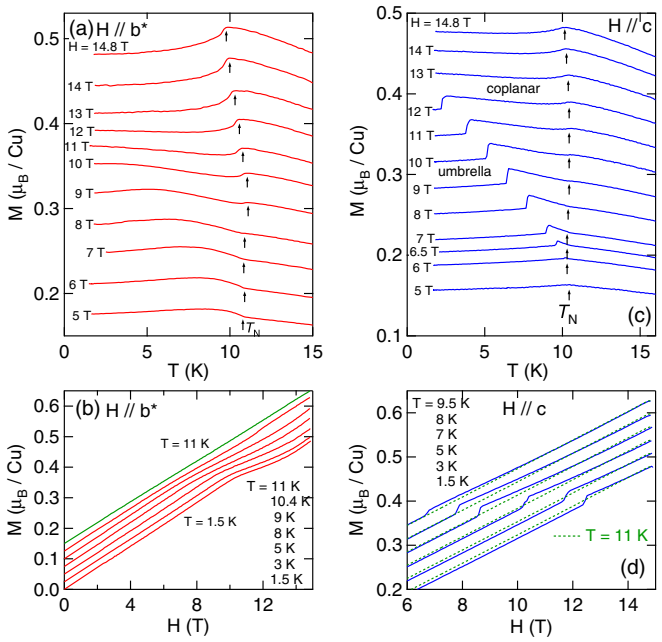

FIG. 9. Temperature dependence of the magnetization of $CsCuCl_3$ for (a) $H \parallel b^*$ and (c) $H \parallel c$ at various magnetic fields up to 14.8 T. Magnetization curves of $CsCuCl_3$ for (b) $H \parallel b^*$ and (d) $H \parallel c$ at various temperatures. The origin of the vertical axis is shifted in each M-H curve.

appears at $T_{u\text{-}c}$ below T_N. $T_{u\text{-}c}$ is the transition temperature from the umbrella to the 2-1-coplanar phase. At $T_{u\text{-}c}$, a sharp jump ΔM is observed and $T_{u\text{-}c}$ decreases rapidly with increasing magnetic field. As is shown in Fig. 9(d), the M-H curve exhibits a jump ΔM at $H_{u\text{-}c}$.

Figures 10(a) and 10(b) represent the magnetic phase diagrams of $CsCuCl_3$ for $H \parallel b^*$ and $H \parallel c$, respectively. The present results are the same as those reported previously [13,28] except the existence of IC4 phase for $H \parallel b^*$. For $H \parallel b^*$, the low field and plateau region were called as IC1 and IC3 phases, respectively. T_N slightly increases with

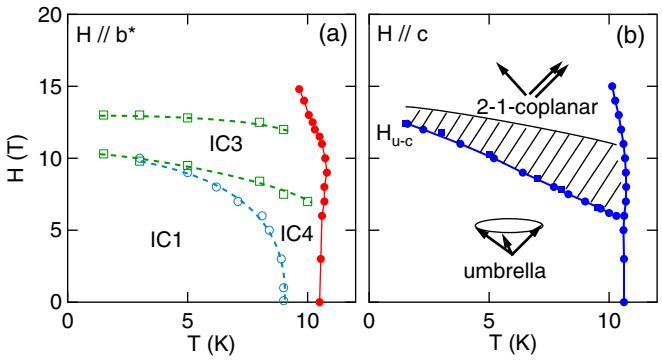

FIG. 10. (a) Magnetic phase diagram of $CsCuCl_3$ for $H \parallel b^*$. Red and blue circles are plotted from the temperature dependence of magnetization and green squares are from magnetic field dependence of magnetization. See the text in details. (b) Magnetic phase diagram for $H \parallel c$. In the hatched area, T_N increases with increasing magnetic field, which might be due to the larger effect of the thermal and quantum spin fluctuation than the Zeeman effect.

increasing magnetic field up to ~8 T and decreases above ~9 T. T_{max} below T_N decreases with increasing magnetic field as is shown by blue open circles and coincides with the IC1-IC3 boundary at the lowest temperature. On the other hand, although the magnetic field of a shoulder decreases with increasing temperature, it is a finite value of ~6 T at T_N. Here, we call the region between IC1 and IC3 phase below T_N as IC4 phase as is shown in Fig. 10(a).

On the other hand, for $H \parallel c$, the first-order phase transition accompanied with a jump ΔM exists between the umbrella and the 2-1-coplanar phases as is shown in Fig. 10(b). Although T_N in the umbrella phase decreases with increasing magnetic field, T_N in the 2-1-coplanar phase increases slightly between 6 and 8 T. This might originate from the enhancement of the thermal and quantum spin fluctuations with increasing magnetic field. $H_{u\text{-}c}$ exhibits a large-T dependence in contrast to the T-independent one in $Ba_3CoSb_2O_9$.

IV. DISCUSSION

A. Analysis of the anisotropy of the magnetization of $Ba_3CoSb_2O_9$ by the mean field calculation

The Co^{2+} ion in $Ba_3CoSb_2O_9$ is dominated by the crystalline electric field, mainly cubic but with a small trigonal component and also the spin-orbit (SO) coupling. The magnetic properties of Co^{2+} ion in such circumstance were previously studied in details [38–40]. The total orbital and spin angular momenta are $L = 3$ and $S = \frac{3}{2}$, respectively. The ground state in a cubic crystalline electric field is a triplet $^4T_1$. The degeneracy of the 12 states in $^4T_1$ is lifted by the SO coupling and trigonal crystalline electric field.

In order to obtain the information on the anisotropy of the g factor and exchange interaction in $Ba_3CoSb_2O_9$, we analyzed the anisotropy of the magnetization at high temperatures and high magnetic fields by the mean field calculation for the three-sublattice model. The Hamiltonian consists of the SO coupling, uniaxial crystalline electric field, Zeeman and exchange interactions [38–40]. Here, we note that the exchange interaction used in the present analysis is isotropic. However, anisotropy of the g factor and the exchange interaction appears in the ground state through the orbital moment of Co^{2+} ion:

$$\mathcal{H} = \mathcal{H}_{SO} + \mathcal{H}_{crys} + \mathcal{H}_{Zeeman} + \mathcal{H}_{ex}, \tag{1}$$

$$\mathcal{H}_{SO} = -\frac{3}{2}\lambda' \boldsymbol{l} \cdot \boldsymbol{S}, \tag{2}$$

$$\mathcal{H}_{crys} = -\delta\left(l_z^2 - \frac{2}{3}\right), \tag{3}$$

$$\mathcal{H}_{Zeeman} = \left(-\frac{3}{2}k\boldsymbol{l} + 2\boldsymbol{S}\right)\mu_B \cdot \boldsymbol{H}, \tag{4}$$

$$\mathcal{H}_{ex} = -J_{ex}\sum_{ij} \boldsymbol{S}_i \cdot \boldsymbol{S}_j. \tag{5}$$

Here, $\lambda' = k\lambda$. λ and δ are the strength of the SO coupling and the uniaxial crystalline electric field, respectively. k is the parameter reflecting the magnitude of the admixture between $3d$ electron of Co^{2+} ion and p electron in ligands. k is less than 1 and is typically ~0.9 [39]. It is known that $\lambda = -180\,\mathrm{cm}^{-1} \sim$

-250 K for Co^{2+} ion [39]. In the case where there exists only the SO coupling, the energy levels of the 12 states are -890.7 K (2), -356.3 K (4), and 534.4 K (6). The number inside the parentheses indicates the degeneracy of the states. Since the first excited states are located 534 K above the ground states, the magnetic properties at low temperatures are dominated by the ground state.

First, we discuss the δ dependencies of the anisotropy of the g factor and the exchange interaction, etc. Here, we follow the formulations by Lines [39]. The ground-state wave functions by the SO coupling are

$$\Psi_+^{(0)} = c_1\left|-1,\tfrac{3}{2}\right\rangle + c_2\left|0,\tfrac{1}{2}\right\rangle + c_3\left|1,-\tfrac{1}{2}\right\rangle, \tag{6a}$$

$$\Psi_-^{(0)} = c_1\left|1,-\tfrac{3}{2}\right\rangle + c_2\left|0,-\tfrac{1}{2}\right\rangle + c_3\left|-1,\tfrac{1}{2}\right\rangle. \tag{6b}$$

Here, when $\delta = 0$, $c_1 = \frac{1}{\sqrt{2}}$, $c_2 = -\frac{1}{\sqrt{3}}$, $c_3 = \frac{1}{\sqrt{6}}$.

The effective exchange interaction in the ground state is expressed by using c_1, c_2, and c_3 in the ground state as follows:

$$\mathcal{H}_{\rm ex}^{(g)} = -J_{\rm ex}\sum_{ij}\left\{q^2\left(S_i^xS_j^x + S_i^yS_j^y\right) + p^2S_i^zS_j^z\right\}, \tag{7}$$

$$p = 3c_1^2 + c_2^2 - c_3^2, \tag{8}$$

$$q = 2\left(\sqrt{3}c_1c_3 + c_2^2\right). \tag{9}$$

The c_1c_3 and c_2^2 terms in Eq. (9) originate from the off-diagonal matrix elements of S^+ or S^- between $|\mp 1, \pm\frac{3}{2}\rangle \leftrightarrow |\mp 1, \pm\frac{1}{2}\rangle$ and $|0,\frac{1}{2}\rangle \leftrightarrow |0,-\frac{1}{2}\rangle$. The anisotropy of the exchange interaction in the ground state is defined as

$$\frac{J}{J_z} = \frac{q^2}{p^2}. \tag{10}$$

In the above effective Hamiltonian (7), the anisotropy of the exchange interaction originates from the wave function of the ground state induced by the SO coupling and the uniaxial crystalline electric field. Here, we note that the definition of p is a factor of 2 different from that by Lines [39].

The g factor consists of the two contributions, i.e., the spin angular momentum (p, q) and the orbital one (p_l, q_l) as follows:

$$g_\parallel = 2\left(3c_1^2 + c_2^2 - c_3^2\right) + 3k\left(c_1^2 - c_3^2\right) \equiv 2p + p_l, \tag{11}$$

$$g_\perp = 4\left(\sqrt{3}c_1c_3 + c_2^2\right) - 3\sqrt{2}kc_2c_3 \equiv 2q + q_l. \tag{12}$$

The $-3\sqrt{2}kc_2c_3$ term in Eq. (12) originates from the off-diagonal matrix element of l^+ or l^- between $|0,\pm\frac{1}{2}\rangle \leftrightarrow |\mp 1,\pm\frac{1}{2}\rangle$. The anisotropy of the g factor is expressed by using p, q, p_l, and q_l as follows:

$$\frac{g_\perp}{g_\parallel} = \frac{2q + q_l}{2p + p_l}. \tag{13}$$

Here, $g_\parallel$ and $g_\perp$ are the g factors for $H \parallel z$ and $H \parallel x$, respectively.

Figures 11(a)–11(d) exhibit the calculated results of the δ dependencies of $|c_i|$, p, q, p_l and q_l, $g_\parallel$ and $g_\perp$, and the anisotropy ratios of the g factor and the exchange interaction, respectively, by assuming $\lambda = -250$ K and $J_{\rm ex} = 0$ K. $|c_i|$, p, q do not depend on the magnitude of k but p_l, q_l, $g_\parallel$, and

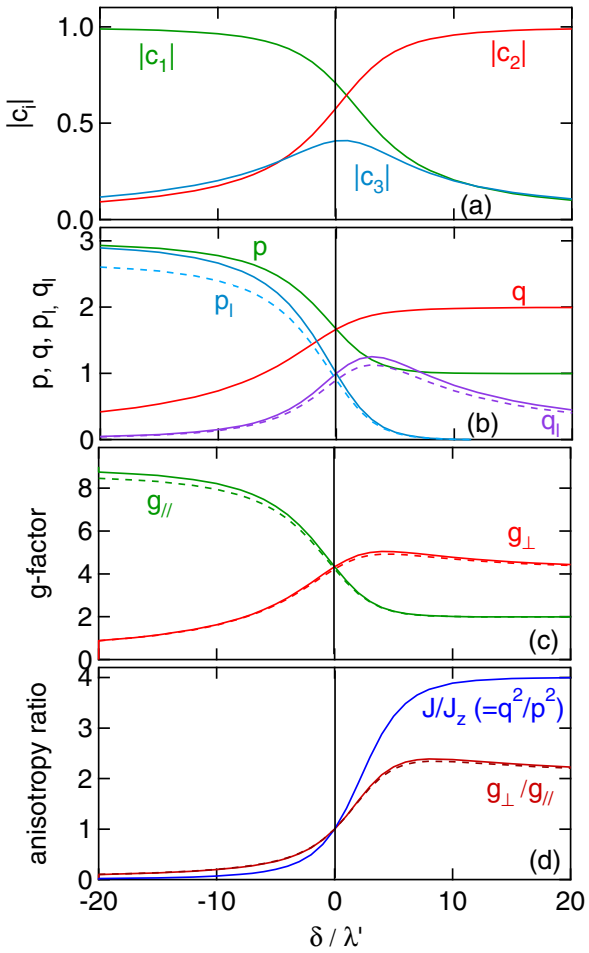

FIG. 11. δ/λ' dependencies of (a) $|c_i|$ $(i = 1, 2, 3)$, (b) p, q, p_l, q_l, (c) $g_\parallel$ and $g_\perp$ for $k = 1$, and (d) anisotropy ratios of J/J_z and $g_\perp/g_\parallel$. Dashed lines in (b), (c), and (d) indicate the results for $k = 0.9$. See the text in details.

$g_\perp$ depend on it because k is included in their formulations. The solid and dashed lines in Figs. 11(b)–11(d) indicate the results for $k = 1$ and 0.9, respectively. For $\delta = 0$, $c_1 = 1/\sqrt{2}$, $c_2 = -1/\sqrt{3}$, and $c_3 = 1/\sqrt{6}$ and in this case, there exists no magnetic anisotropy. However, when a finite magnitude of δ/λ' is introduced, the anisotropy is induced both in the g factor and the exchange interaction. When $\delta/\lambda' > 0$, the easy-plane magnetic anisotropy is enhanced with increasing δ/λ'. When $\delta/\lambda' \to \infty$, $\Psi_\pm^{(0)} \to |0,\pm\frac{1}{2}\rangle$, $(p,q,p_l,q_l) \to (1,2,0,0)$, and $(g_\parallel, g_\perp) \to (2,4)$ where the contribution of the orbital angular momentum disappears. When $\delta/\lambda' < 0$, the uniaxial magnetic anisotropy along the z axis is enhanced with increasing $|\delta/\lambda'|$. When $\delta/\lambda' \to -\infty$, $\Psi_\pm^{(0)} \to |\mp 1,\pm\frac{3}{2}\rangle$, $(p,q,p_l,q_l) \to (3,0,3,0)$, and $(g_\parallel, g_\perp) \to (9,0)$ where there exist the maximum contributions from both l_z and S_z. There, the Ising spin system is realized because there exists no spin-flip transition between $\Psi_+^{(0)}$ and $\Psi_-^{(0)}$. A broad maximum of q_l exists at $\delta/\lambda' \sim 3$. This originates from the orbital contribution of $q_l = -3\sqrt{2}kc_2c_3$, i.e., the product of $|c_2|$ which increases rapidly at $\delta/\lambda' \sim 2$ and $|c_3|$ which shows a broad maximum at $\delta/\lambda' \sim 1$. This broad maximum of q_l is the origin of the broad maximum

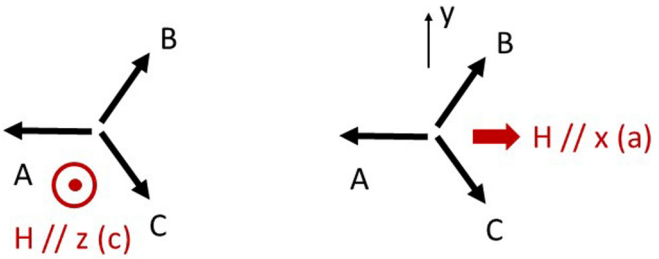

FIG. 12. Three-sublattice model with 120° spin structure in the xy plane at $H = 0$. The antiferromagnetic exchange interaction works between A-B, B-C, and C-A. The magnetic field is applied along the z axis (left) and the x axis (right). z and x axes correspond to c and a axes in $Ba_3CoSb_2O_9$, respectively.

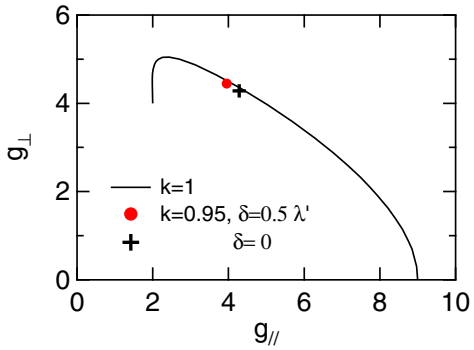

FIG. 13. Relationship between $g_\parallel$ and $g_\perp$. Solid line is that for $k = 1$. Red circle and black plus symbol indicate $g_\perp$ and $g_\parallel$ for $\delta = 0.5\lambda'$ and 0 when $k = 0.95$.

of $g_\perp$ at $\delta/\lambda' \sim 2$. The anisotropy of $g_\perp$ and $g_\parallel$ is reflected in the anisotropic magnetic susceptibility in the paramagnetic region. Figure 11(d) shows the δ/λ' dependence of the anisotropic ratio of J/J_z and $g_\perp/g_\parallel$. When $\delta/\lambda' > 0$, J/J_z is larger than $g_\perp/g_\parallel$ and when $\delta/\lambda' < 0$, J/J_z is smaller than $g_\perp/g_\parallel$. This is because J/J_z is proportional to $(q/p)^2$ but $g_\perp/g_\parallel$ is proportional to $(2q + q_l)/(2p + p_l)$. This ratio is slightly different from $(2q/2p)$ by the angular momentum contributions of p_l and q_l. We comment the validity of the δ/λ' dependence of the physical quantities in Figs. 11(a)–11(d). For $\delta/\lambda' < 0$, the results are correct because the excited states are always well separated from the ground state. However, in the case of $\delta/\lambda' > 0$, especially for $\delta/\lambda' > 10$, those are not necessarily correct because the energy separation between the ground state and the excited one decreases rapidly with increasing δ/λ'.

Now, we analyze the anisotropic magnetization of $Ba_3CoSb_2O_9$ by the mean field calculation for the three-sublattice model. The Hamiltonian consists of the three sublattices of A, B, and C and it is assumed that their spins form a 120° spin structure in the xy plane initially as shown in Fig. 12. The x and z axes correspond to the a and c axes in $Ba_3CoSb_2O_9$, respectively. The exchange interaction works between A-B, B-C, and C-A sublattices. The magnetic field is applied along the z and x axes. The basis of the Hamiltonian consists of 12 wave functions, i.e., $|l_z, S_z\rangle = |\mp 1, \pm\frac{3}{2}\rangle, |0, \pm\frac{1}{2}\rangle, |\pm 1, \mp\frac{1}{2}\rangle, |0, \pm\frac{3}{2}\rangle, |\pm 1, \pm\frac{1}{2}\rangle, |\pm 1, \pm\frac{3}{2}\rangle$. We took $J_{ex} = -18$ K and k and δ are parameters to reproduce the experimental results at high temperatures and at high magnetic fields.

In the mean field calculation for the three-sublattice model, the Hamiltonian for the A sublattice is written as follows:

$$\mathcal{H} = \sum_{i\in A} h_i^A + \sum_{i\in B} h_i^B + \sum_{i\in C} h_i^C, \tag{14}$$

$$h_i^A = -\frac{3}{2}\lambda' \boldsymbol{l}_i \cdot \boldsymbol{S}_i - \delta\left(\left(l_i^z\right)^2 - \frac{2}{3}\right) + \left(-\frac{3}{2}k\boldsymbol{l}_i + 2\boldsymbol{S}_i\right)\mu_B \cdot \boldsymbol{H} - J_{ex}\left\{(\langle S_x\rangle^B + \langle S_x\rangle^C)S_i^x + (\langle S_y\rangle^B + \langle S_y\rangle^C)S_i^y + (\langle S_z\rangle^B + \langle S_z\rangle^C)S_i^z\right\}. \tag{15}$$

The Hamiltonians for the B and C sublattices are written in the same manner. Here, we note that although there exists the anisotropic exchange interaction in the effective Hamiltonian by Lines [39], the isotropic exchange interaction is used in the present calculation. This is because in the Lines's model [39], the anisotropic exchange interaction is introduced by the wave function of the ground state well separated from the excited states. On the other hand, in the present numerical calculation, all the excited states are taken into account. Then, the T and H dependencies of the anisotropy of both anisotropic exchange interaction and g factor are induced.

First, the mean field calculation was performed to reproduce the anisotropic magnetic susceptibility of $Ba_3CoSb_2O_9$ at high temperatures and we obtain $k = 0.95$ and $\delta/\lambda' = 0.5$ by assuming $\lambda = -250$ K and $J_{ex} = -18$ K. The calculated energy levels of the 12 states at $H = 0$ without the exchange interaction are -893.3 K (2), -391.6 K (2), -324.6 K (2), 505.4 K (2), 530.1 K (2), and 574.0 K (2). In this case, $g_\parallel = 3.952$ and $g_\perp = 4.447$ are obtained and these indicate a large easy-plane magnetic anisotropy. Figure 13 shows the relationship between $g_\perp$ and $g_\parallel$. The solid line is that for $k = 1$ and the red circle indicates that for $\delta/\lambda' = 0.5$ with $k = 0.95$ and black plus symbol that for $\delta = 0$. When $k = 0.95$ and $\delta = 0$, the g factor is isotropic and $g_\parallel = g_\perp = 4.28 \equiv g$. Since the ratio of $g_\parallel(k = 0.95)/g$ is 0.923 and $g_\perp(k = 0.95)/g$ is 1.04, the effect of δ is larger in $g_\parallel$ than in $g_\perp$.

The calculated χ and χ^{-1}, shown in Figs. 14(a) and 14(b), respectively, reproduce well the experimental results above 100 K. The magnetic anisotropy in the paramagnetic region is large and the Curie-Weiss behavior is seen down to 150 K. These are consistent with the experimental results in the same temperature region. The large deviations from the calculated results below ~100 K are due to the SRO effect originating from the large two-dimensional spin fluctuation in $Ba_3CoSb_2O_9$. The calculated T_N is 14 K, which is much higher than $T_N = 3.8$ K of $Ba_3CoSb_2O_9$, which originates from the suppression of the AFM interaction by the two-dimensional AFM spin fluctuation.

Next, we discuss the M-H curves within a framework of the mean field calculation. Figure 15(a) shows the calculated M-H curves for $H \parallel x$ and $H \parallel z$ at $T = 0$ K by using $\delta = 0.5\lambda'$ and $k = 0.95$ obtained by the fitting of χ at high temperatures. The black dotted line displays the M-H curve for $H \parallel z$ in the case of $\delta = 0$. In this case, the M-H curve shows the H-linear increase in the umbrella phase, which originates from the spin-canting magnetization process and the saturation field $H_s = 27.7$ T. The magnetic anisotropy appears when the finite magnitude of δ is introduced. A positive δ induces the easy-

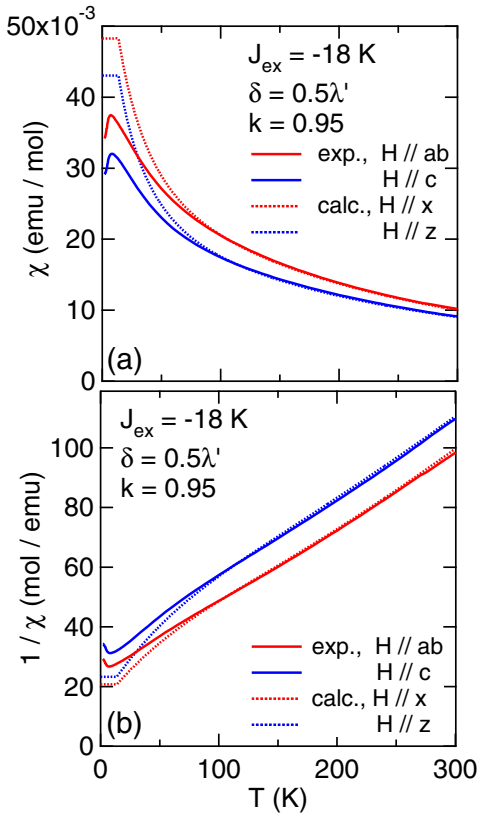

FIG. 14. Temperature dependence of (a) magnetic susceptibility and (b) inverse magnetic susceptibility of $Ba_3CoSb_2O_9$ for $H \parallel ab$ and $H \parallel c$. Dotted lines are the calculated results for the three-sublattice model for $H \parallel x$ and $H \parallel z$ by using the parameters of $\delta = 0.5\lambda'$, $k = 0.95$, and $J_{ex} = -18$ K. See the text in details.

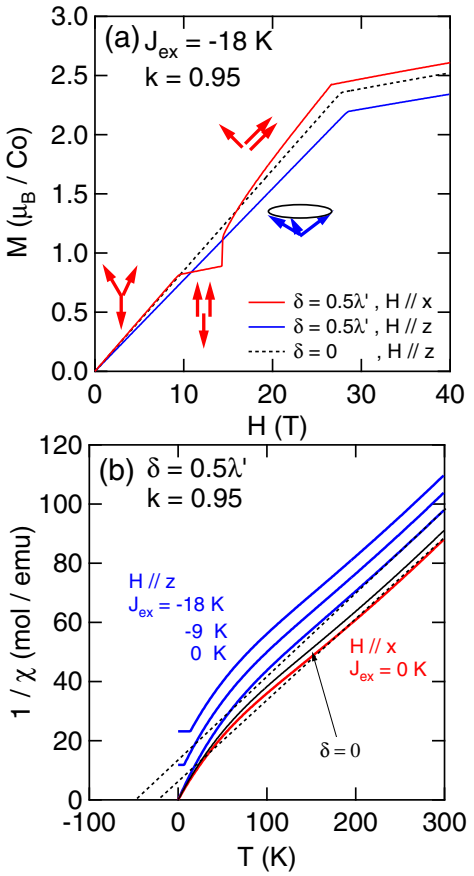

FIG. 15. (a) Magnetization curves for $H \parallel x$ and $H \parallel z$ in the three-sublattice model with $\delta = 0.5\lambda'$ and $J_{ex} = -18$ K at $T = 0$ K calculated by the mean field approximation. The black dotted line indicates the calculated one with $\delta = 0$ for $H \parallel z$. (b) Temperature dependence of the inverse magnetic susceptibilities for $H \parallel x$ and $H \parallel z$ in the three-sublattice model with $\delta = 0.5\lambda'$. For $H \parallel z$, the results with $J_{ex} = -18$ K, -9 K, and 0 and for $H \parallel z$, that with $J_{ex} = 0$ K are shown. Black solid line indicates the result with $\delta = 0$ for $H \parallel x$. The black dotted lines are drawn to estimate the paramagnetic Curie temperature θ_p. See the text for details.

plane magnetic anisotropy, i.e., $M_x > M_z$, and a negative δ the uniaxial magnetic anisotropy along the z axis, $M_z > M_x$.

In the present calculation for $H \parallel x$, there appear the Y-, *uud*- and 2-1-coplanar phases. However, we should be careful to discuss the results because the effect of the quantum spin fluctuation which is well known to play an essential role in the ordered phase in the TLA compounds. For example, there exist the following problems. Although the results are self-consistent solutions, in the 2-1-coplanar phase, the three spins are located not in the xy plane but in the zx planes. In this case, there exists a large energy loss of the magnetic anisotropy. Furthermore, when the applied H is only slightly deviated from the x direction in the xy plane, the *uud* phase disappears and in the 2-1-coplanar phase, the three spins are located in the xy plane. The smooth continuous phase transition from the Y-coplanar to the *uud* phase and the first one from the *uud* to the 2-1-coplanar one appear also for $\delta = 0$. It is well known that the *uud* phase appears only taking the quantum spin fluctuation into account. For $H \parallel z$, there exists only the umbrella phase. This is not correct. It is well known that the first-order phase transition from the umbrella to the 2-1-coplanar phase exists when the quantum spin fluctuation is taken into account. Thus, the results by the mean field calculation are not reliable to discuss the AFM ordered phases. However, at high magnetic field above H_s in the paramagnetic region, the important information on the anisotropy could be obtained.

H_s for $H \parallel x$ is smaller than that for $H \parallel z$, reflecting the magnetic anisotropy. The anisotropy ratio of M_x/M_z at $H = 30$ T is 1.12, which is almost the same value as that of χ_x/χ_z at high temperatures. The anisotropy of the high-field magnetization at low temperature and the anisotropic magnetic susceptibility at high temperatures are directly related to each other because both regions are paramagnetic. It is noted that the calculated H_s is not far from the experimental value of $\sim$32 T [32]. The slightly small value of the calculated H_s could be enhanced by introducing the small magnitude of the AFM interaction within the same sublattice.

A large van Vleck contribution exists above H_s in the M-H curve. The slope of M-H curve above H_s is $\sim 1.25 \times 10^{-2} \mu_B/\mathrm{T/Co^{2+}}$ which is slightly smaller than the previously reported value of 1.59×10^{-2} for $H \parallel ab$ and 1.90×10^{-2} for $H \parallel c$ [32].

Figure 15(b) represents the T dependence of χ^{-1} for $H \parallel x$ and $H \parallel z$ in the case of $\delta = 0.5\lambda'$. In this figure, those with different magnitudes of the exchange interaction are also shown for $H \parallel z$; only the results with $J_{ex} = 0$ are shown for $H \parallel x$. The black solid line shows that with $\delta = 0$ and $J_{ex} = 0$. By introducing the finite magnitude of δ, the anisotropy appears. Then, even in the case of $J_{ex} = 0$, the finite magnitude of θ_p appears and is estimated to be ~ -20 K and ~ -50 K for $H \parallel x$ and $H \parallel z$, respectively. Of course, these never originate from the exchange interaction. The real θ_p is estimated from the negative shift from that of $J_{ex} = 0$ as is seen for the blue lines with negative values of J_{ex} in Fig. 15(b).

When $\delta = 0.5\lambda'$ and $k = 0.95$, the following values of p, q, p_l, q_l, $g_\parallel$, and $g_\perp$ are obtained by using the obtained values of c_1, c_2, and c_3:

$$p = 1.5705, \quad q = 1.7133, \quad p_l = 0.8107, \quad q_l = 1.0199,$$
$$g_\parallel = 2p + p_l = 3.9517, \quad g_\perp = 2q + q_l = 4.4465.$$

We note that the anisotropy of g factor is larger than the previously reported ones [32]. From the above values, the anisotropy ratios of the exchange interaction and g factor are estimated as follows:

$$J/J_z = q^2/p^2 = 1.190, \quad g_\perp/g_\parallel = 1.125.$$

The anisotropic ratio of $J/J_z = 1.19$ is comparable to those used in the theoretical analyses. It is close to 1.25 by Yamamoto *et al.* [35] and 1.123 by Ma *et al.* [37]. We believe that the present results are reliable because they are obtained from the magnetization at high temperatures and high fields, which are not affected by the quantum spin fluctuation. Thus, we could obtain the important information on the anisotropy of the exchange interaction and the g factor. In this paper, we used the simple Hamiltonian (1), where we assume the isotropic Heisenberg exchange interaction as the simplest case. Then, the physical meaning of the calculated results is clearly understood. Although it is possible to introduce the anisotropy in the exchange interaction phenomenologically in the Hamiltonian (5), it will be difficult to understand the physical meaning of the calculated results. In the theoretical analysis, it is important to estimate the anisotropy of the exchange interaction correctly. In the previous studies, the anisotropy of the g factor and that of the exchange interaction were estimated independently. However, in the present calculation, we showed that although the isotropic exchange interaction is used, the anisotropy of the g factor and the exchange interaction are introduced in the ground state obtained by the SO interaction and the uniaxial crystalline electric field. Furthermore, the anisotropy of the g factor and that of the exchange interaction are not independent because both are calculated by the same values of c_1, c_2, and c_3 in the ground state. The orbital degrees of freedom is introduced simultaneously both in the g factor and the exchange interaction in the ground state through the van Vleck term from the excited states. The van Vleck contribution is not small as shown in the present calculation. Thus, in the compound including the Co^{2+} ion, the orbital degrees of freedom should be considered seriously.

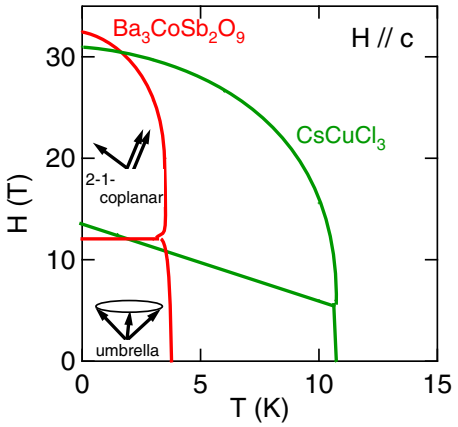

FIG. 16. Schematic magnetic phase diagrams of $Ba_3CoSb_2O_9$ (red line) and $CsCuCl_3$ (green line) for $H \parallel c$. See the text in details.

B. Effect of the interplane interaction on the AFM order

Both $Ba_3CoSb_2O_9$ and $CsCuCl_3$ are the TLA with $S = \frac{1}{2}$. However, there exist several large differences. Figure 16 represents the schematic magnetic phase diagrams of $Ba_3CoSb_2O_9$ and $CsCuCl_3$ for $H \parallel c$. In the former, the magnetic phase diagram in high-field region is not known at present, while that up to 16 T was reported [33]. The saturation field H_s is known to be 32.8 T [32]. Here, we assume that only the 2-1-coplanar phase exists between 12.5 and 32.8 T. The magnetic phase diagram of $CsCuCl_3$ was reported by Nojiri *et al.* [13]. Although H_s is nearly the same, T_N is very different between these two compounds. T_N is 3.8 and 10.7 K in $Ba_3CoSb_2O_9$ and $CsCuCl_3$, respectively. The former is only one third of the latter. Another difference is the T dependence of χ in the paramagnetic region as was mentioned in Sec. III. In the $Ba_3CoSb_2O_9$, a broad maximum exists above T_N, originating from the two-dimensional spin fluctuation. On the other hand, in $CsCuCl_3$, such a maximum does not exist and χ in the paramagnetic region exhibits a Curie-Weiss behavior in a wide range of temperature.

As was mentioned in the Introduction, there exists a large difference in the nature of the exchange interaction. It originates from the difference of the crystal structures. In $Ba_3CoSb_2O_9$, the triangular-lattice plane is separated by the nonmagnetic atoms in the intervening plane and the distance between the magnetic planes is large. Due to this crystal structure, the quasi-two-dimensional triangular lattice is realized. This low dimensionality enhances the spin fluctuation in the paramagnetic region and suppresses T_N down to 3.8 K. In $CsCuCl_3$, the Cu-Cl-Cu bond angle close to 90° along the c axis and the short distance between the triangular-lattice magnetic planes make the exchange interaction along the c axis ferromagnetic and strong. This FM interaction J_{ex}^c is as large as 28 K. On the other hand, the in-plane AFM interaction is small, $J_{ex}^{ab} \sim -5$ K. Due to the strong FM interaction along the c axis, although the AFM order takes a 120° spin structure in the ab plane, the three-dimensional nature is contained. Of course, this is not the usual three-dimensional magnetic order but the TLA order which is constructed by the strong one-dimensional FM chains. The DM interaction works between the spins located in the nearest-neighbor planes along the c axis. This

also enhances the three-dimensional magnetic order. We note that in $CsCuCl_3$, $T_N = 10.7$ K is higher than the in-plane AFM exchange interaction of ~5 K. This high T_N could be assisted by the strong one-dimensional FM chain along the c axis. Namely, the strongly coupled one-dimensional FM chain could construct more easily the three-dimensional AFM order.

C. Thermal and quantum spin fluctuations and DM interaction

Here, we discuss the different nature of the magnetic anisotropy and thermal and quantum spin fluctuations between $Ba_3CoSb_2O_9$ and $CsCuCl_3$.

1. $H \parallel c$

As is shown in Fig. 16, there exists a large difference in the T dependence of $H_{u\text{-}c}$ for $H \parallel c$. In $Ba_3CoSb_2O_9$, $H_{u\text{-}c}$ is almost independent of temperature. On the other hand, it strongly depends on the temperature in $CsCuCl_3$. In the umbrella phase, T_N is suppressed by magnetic field as in a usual antiferromagnet. This is because in the umbrella phase, the thermal and quantum spin fluctuations are small. On the other hand, T_N in the coplanar phase is enhanced with increasing magnetic field, although it is small. In $Ba_3CoSb_2O_9$, the suppression of T_N is observed in a narrow field region between 12 and 13 T. In $CsCuCl_3$, in a rather wide field region between 6 and 10 T as shown by the hatched area in Figs. 5(b) and 10(b), respectively. In this magnetic field region, M_c exhibits an increase with decreasing temperature below T_N. $dT_N/dH > 0$ and $dM_c/dT < 0$ below T_N are induced by the enhancement of the thermal and quantum spin fluctuations by magnetic field. Namely, the thermal and quantum spin fluctuations are enhanced in the hatched area in these figures. The hatched area is very different between the two compounds. It is narrow and almost parallel to $H_{u\text{-}c}$ in $Ba_3CoSb_2O_9$, but it is wide and expanded with increasing temperature in $CsCuCl_3$. This difference might originate from the different magnitude of the easy-plane magnetic anisotropy.

The temperature independent $H_{u\text{-}c}$ in $Ba_3CoSb_2O_9$ means that the difference of the magnetic entropy below and above $H_{u\text{-}c}$ is very small. This indicates that the thermal and quantum spin fluctuations in the coplanar phase in $Ba_3CoSb_2O_9$ are small as in the umbrella phase. In $Ba_3CoSb_2O_9$, the easy-plane magnetic anisotropy is rather strong in the paramagnetic region and remains also in the AFM ordered state. It is because a large contribution of the orbital momentum of Co^{2+} ion should be associated with the origin of the easy-plane magnetic anisotropy below and above T_N as is discussed in the previous Sec. III A. In such a situation, the spin canting from the ab plane for $H \parallel c$ loses a large energy gain by the easy-plane magnetic anisotropy. This suppresses the thermal and quantum spin fluctuations for $H \parallel c$. On the other hand, for $H \parallel ab$, the thermal and quantum spin fluctuations are active because the energy gain by the easy-plane magnetic anisotropy is always obtained.

In $CsCuCl_3$, $H_{u\text{-}c}$ decreases considerably with increasing temperature. This large slope of $H_{u\text{-}c}/T$ means that the magnetic entropy in the coplanar phase is larger than that in the umbrella one. This indicates that the thermal and quantum spin fluctuations in the coplanar phase are stronger than those in the umbrella phase. The large-T dependence of $H_{u\text{-}c}$ in $CsCuCl_3$ indicates that the easy-plane magnetic anisotropy energy gain is reduced with increasing temperature. Namely, in the AFM state, the higher the temperature, the smaller the easy-plane magnetic anisotropy energy gain. Then, the energy loss of the magnetic anisotropy induced by the spin canting from the ab plane is reduced with increasing temperature. This occurs in the hatched area in Fig. 10(b). As the origin of the T-dependent easy-plane magnetic anisotropy, the DM interaction is considered. Its strength depends on the temperature because it is proportional to $|\boldsymbol{S}_i \times \boldsymbol{S}_j|$, where $\boldsymbol{S}_i$ and $\boldsymbol{S}_j$ are the spins located in the ab plane and $|\boldsymbol{S}_i \times \boldsymbol{S}_j| \propto |S_{(x,y)}|^2$ for $\boldsymbol{D} \parallel c$. $S_{(x,y)}$ is the magnitude of the spin located in the ab plane. Its magnitude is the largest at $T = 0$ K and decreases with increasing temperature. Then, the magnitude of the easy-plane magnetic anisotropy is reduced with increasing temperature. This might be the origin of the large-T dependence of $H_{u\text{-}c}$ in $CsCuCl_3$. This situation is, in some sense, similar to the calculated results for the model with the uniaxial magnetic anisotropy $D\sum_i (S_i^z)^2$ by Watari *et al.* [6]. Thus, we propose that the different T dependence of $H_{u\text{-}c}$ for $H \parallel c$ between $Ba_3CoSb_2O_9$ and $CsCuCl_3$ originates from the different nature of the easy-plane magnetic anisotropy and its T dependence. Namely, in $Ba_3CoSb_2O_9$, the magnetic anisotropy is dominated by the large orbital momentum of Co^{2+} ion both below and above T_N. In $CsCuC_3$, it is dominated by the DM interaction which enhances the easy-plane magnetic anisotropy with decreasing temperature below T_N.

2. $H \parallel ab$

For $H \parallel ab$, since the spins are always located in the ab plane, there is no competition between the easy-plane magnetic anisotropy and Zeeman interaction. Then, we only have to consider the competition or coexistence of the thermal and quantum spin fluctuations and Zeeman interaction. In $Ba_3CoSb_2O_9$, a pronounced enhancement of T_N is observed up to 13 T. This clearly indicates that the uud state is stabilized by getting the thermal and quantum spin fluctuation energy gain induced by magnetic field. On the other hand, in $CsCuCl_3$, the enhancement of T_N with increasing magnetic field is very small. This small enhancement of T_N is due to the spiral magnetic order along the c axis. This originates from the DM interaction and suppresses the thermal and quantum spin fluctuations. The reason why the clear phase boundary does not exist in $CsCuCl_3$ below T_N is also due to the existence of the DM interaction. As a function of temperature, a broad maximum of χ_{ab} at T_{max} might correspond to $T_{Y\text{-}uud}$ in $Ba_3CoSb_2O_9$ and as a function of H, a broad shoulder at $H \sim 9.5$ T corresponds to $H_{Y\text{-}uud}$. Thus, for $H \parallel b^*$ in $CsCuCl_3$, the competition between the thermal and quantum spin fluctuations and DM interaction in magnetic field makes the clear transition difficult and in place, a broad crossover appears.

V. CONCLUSION

We have investigated the magnetization of the $S = \frac{1}{2}$ TLA, $Ba_3CoSb_2O_9$, and $CsCuCl_3$ in details. These two compounds exhibit very different magnetic properties, although the thermal and quantum spin fluctuations play the important role in both compounds.

$Ba_3CoSb_2O_9$ was considered as the ideal TLA. On the other hand, the AFM state in $CsCuCl_3$ is considerably modified by the strong FM and DM interactions along the c axis. Although $H_s \sim 30$ T is nearly the same in both compounds, T_N of the former is much smaller than that of the latter. Although χ in the former exhibits a broad maximum above T_N, that in the latter exhibits a continuous increase down to T_N. These differences originate from the difference of the crystal structure giving rise to very different nature of the exchange interaction. In the former, the interplane AFM interaction is very weak, but in the latter there exist the strong FM and DM interactions along the c axis. The strong FM interaction along the c axis dominates the magnetic properties in the paramagnetic region and also makes the three-dimensional AFM order easier.

The magnetic phase diagrams are very different between $Ba_3CoSb_2O_9$ and $CsCuCl_3$. For $H \parallel c$, $H_{u\text{-}c}$ is almost independent of the temperature up to T_N in $Ba_3CoSb_2O_9$. On the other hand, in $CsCuCl_3$, it exhibits a considerable decrease with increasing temperature. In $Ba_3CoSb_2O_9$, a large easy-plane magnetic anisotropy exists both below and above $\sim T_N$, which is dominated by the large orbital momentum of the Co^{2+} ion. This suppresses the thermal and quantum spin fluctuations along the c axis. This makes the difference of the magnetic entropy below and above $H_{u\text{-}c}$ small and makes the roughly constant $H_{u\text{-}c}$ in this compound. In $CsCuCl_3$, although there exists an easy-plane magnetic anisotropy as in $Ba_3CoSb_2O_9$, it is small and its main origin is the DM interaction whose magnitude decreases with increasing temperature. This suppresses $H_{u\text{-}c}$ with increasing temperature. For $H \parallel ab$, in both compounds, the spins are located in the ab plane. In such a case, the thermal and quantum spin fluctuations are active in the ab plane. In $Ba_3CoSb_2O_9$, the enhancement of T_N by the thermal and quantum spin fluctuation is clearly seen in the uud phase. Namely, the pronounced reentrant behavior of T_N is observed in the uud phase. On the other hand, in $CsCuCl_3$, the reentrant behavior of T_N in the IC3 phase is much less pronounced. This is due to the existence of the DM interaction, which competes with the Zeeman interaction and suppresses the thermal and quantum spin fluctuations. Furthermore, due to the DM interaction, the clear phase transition does not appear for $H \parallel b^*$ but in place, only broad crossover is observed.

We analyzed the magnetization of $Ba_3CoSb_2O_9$ at high temperatures and high magnetic fields to obtain the information on the anisotropy of the exchange interaction and g factor by the mean field calculation for the three-sublattice model. We determined the uniaxial crystalline electric field so as to fit the anisotropic magnetic susceptibility at high temperatures. Thereby, the anisotropies of the exchange interaction and g factor were obtained simultaneously. The obtained anisotropies are $J/J_z = 1.19$ and $g_\perp/g_\parallel = 1.13$ with $g_\parallel = 3.95$ and $g_\perp = 4.45$. The former is consistent with the recent theoretical studies [35,37]. By using the obtained parameters, we calculated the M-H curve. The high magnetic field M-H curve is consistent with the present experimental result. It is emphasized that the anisotropies of both g factor and exchange interaction originate from the orbital momentum of Co^{2+} ion through the SO coupling and the uniaxial crystalline electric field and they should be determined simultaneously.

ACKNOWLEDGMENTS

The authors would like to thank Professor M. Kurmoo for the stimulating discussion. The authors acknowledge the support from the Japan Society for the Promotion of Science (JSPS) Grant-Aid Scientific Research (S) (Grant No. 25220803) "Towards a New Class Magnetism by Chemistry-controlled Chirarity," the JSPS Grant-Aid for Scientific Research (C) (Grant No. 26400368), the JSPSGrant-AId for Scientific Research on Innovative Areas (Grant No. 15H05885), and the Center for Chiral Science in Hiroshima University (the Ministry of education, Culture, Sports, Science and Technology (MEXT) program for promoting the enhancement of research universities, Japan).

[1] P. W. Anderson, Mater. Res. Bull. **8**, 153 (1973).
[2] L. Balents, Nature (London) **464**, 199 (2010).
[3] H. Kawamura, J. Phys. Soc. Jpn. **53**, 2452 (1984).
[4] H. Kawamura and S. Miyashita, J. Phys. Soc. Jpn. **54**, 4530 (1985).
[5] A. V. Chubukov and D. I. Golosov, J. Phys. C: Solid State Phys. **3**, 69 (1991).
[6] S. Watarai, S. Miyashita, and H. Shiba, J. Phys. Soc. Jpn. **70**, 532 (2001).
[7] S. Miyashita, Proc. Jpn. Acad. Ser. B **86**, 643 (2010).
[8] D. Yamamoto, G. Marmorini, and I. Danshita, Phys. Rev. Lett. **112**, 127203 (2014).
[9] T. Ono, H. Tanaka, H. Aruga Katori, F. Ishikawa, H. Mitamura, and T. Goto, Phys. Rev. B **67**, 104431 (2003).
[10] N. A. Fortune, S. T. Hannahs, Y. Yoshida, T. E. Sherline, T. Ono, H. Tanaka, and Y. Takano, Phys. Rev. Lett. **102**, 257201 (2009).
[11] C. Griset, S. Head, J. Alicea, and O. A. Starykh, Phys. Rev. B **84**, 245108 (2011).
[12] M. Motokawa, Annual Meeting of Physical Society of Japan, 1978 (unpublished).
[13] H. Nojiri, Y. Tokunaga, and M. Motokawa, J. Phys. (Paris) **49**, C8-1459 (1988).
[14] T. Nikuni and H. Shiba, J. Phys. Soc. Jpn. **62**, 3268 (1993).
[15] C. J. Croese, J. C. M. Tindemans-van Eyndhoven, and W. J. A. Masakant, Solid State Commun. **9**, 1707 (1971).
[16] S. Hirotsu, J. Phys. C: Solid State Phys. **10**, 967 (1977).
[17] N. Achiwa, J. Phys. Soc. Jpn. **27**, 561 (1969).
[18] K. Adachi, N. Achiwa, and M. Mekata, J. Phys. Soc. Jpn. **49**, 545 (1980).
[19] H. Hyodo, K. Ito, and K. Nagata, J. Phys. Soc. Jpn. **49**, 545 (1980).
[20] Y. Tazuke, H. Tanaka, K. Iio, and K. Nagata, J. Phys. Soc. Jpn. **50**, 3919 (1981).
[21] H. Tanaka, U. Shotte, and K. D. Shotte, J. Phys. Soc. Jpn. **61**, 1344 (1992).
[22] R. Bugel, A. Faisst, H. v. Loneysen, J. Wosnitza, and U. Shotte, Phys. Rev. B **65**, 052402 (2001).

[23] H. Nojiri, K. Takahashi, T. Fukuda, M. Fujita, M. Arai, and M. Motokawa, Phys. B (Amsterdam) **241**, 210 (1998).
[24] N. Stusser, U. Shotte, A. Hoser, M. Meschke, M. Meissner, and J. Wosnitza, J. Phys.: Condens. Matter **14**, 5161 (2002).
[25] A. E. Jacobs, T. Nikuni, and H. Shiba, J. Phys. Soc. Jpn. **62**, 4066 (1993).
[26] T. Nikuni and A. E. Jacobs, Phys. Rev. B **57**, 5205 (1998).
[27] Y. Kousaka, H. Ohsumi, T. Komesu, T. Arima, M. Takata, S. Sakai, M. Akita, K. Inoue, T. Yokobori, Y. Nakano, E. Kaya, and J. Akimitsu, J. Phys. Soc. Jpn. **78**, 123601 (2009).
[28] A. Miyake, J. Shibuya, M. Akaki, H. Tanaka, and M. Tokunaga, Phys. Rev. B **92**, 100406 (2015).
[29] Y. Doi, Y. Hinatsu, and K. Ohoyama, J. Phys.: Condens. Matter **16**, 8923 (2004).
[30] Y. Shirata, H. Tanaka, A. Matsuo, and K. Kindo, Phys. Rev. Lett. **108**, 057205 (2012).
[31] H. D. Zhou, C. Xu, A. M. Hallas, H. J. Silverstein, C. R. Wiebe, I. Umegaki, J. Q. Yan, T. P. Murphy, J.-H. Park, Y. Qiu, J. R. D. Copley, J. S. Gardner, and Y. Takano, Phys. Rev. Lett. **109**, 267206 (2012).
[32] T. Susuki, N. Kurita, T. Tanaka, H. Nojiri, A. Matsuo, K. Kindo, and H. Tanaka, Phys. Rev. Lett. **110**, 267201 (2013).
[33] G. Quirion, M. Lapointe-Major, M. Poirier, J. A. Quilliam, Z. L. Dun, and H. D. Zhou, Phys. Rev. B **92**, 014414 (2015).
[34] K. Naruse, T. Kawamata, M. Ohno, Y. Matsuoka, H. Sudo, H. Nagasawa, Y. Hagiya, T. Sasaki, and Y. Koike, J. Phys.: Conf. Ser. **568**, 042014 (2014).
[35] D. Yamamoto, G. Marmorini, and I. Danshita, Phys. Rev. Lett. **114**, 027201 (2015).
[36] G. Koutroulakis, T. Zhou, Y. Kamiya, J. D. Thompson, H. D. Zhou, C. D. Batista, and S. E. Brown, Phys. Rev. B **91**, 024410 (2015).
[37] J. Ma, Y. Kamiya, Tao Hong, H. B. Cao, G. Ehlers, W. Tian, C. D. Batista, Z. I. Dun, H. D. Zhou, and M. Matsuda, Phys. Rev. Lett. **116**, 087201 (2016).
[38] A. Abragam and M. H. L. Pryce, Proc. R. Soc. A **206**, 173 (1951).
[39] M. E. Lines, Phys. Rev. **131**, 546 (1963).
[40] H. Shiba, Y. Ueda, K. Okunishi, S. Kimura, and K. Kindo, J. Phys. Soc. Jpn. **72**, 2326 (2003).